Kerr effect in multilayer dielectric coatings

ELENA FEDULOVA,[1,2] MICHAEL TRUBETSKOV,[1] TATIANA AMOTCHKINA,[1] KILIAN FRITSCH,[2] PETER BAUM,[1,2] OLEG PRONIN,[1] AND VLADIMIR PERVAK[2,3,*]

[1]*Max Planck Institute of Quantum Optics, Hans-Kopfermann Str. 1, 85748, Garching, Germany*
[2]*Ludwig Maximilians University, Am Coulombwall 1, 85748, Garching, Germany*
[3]*Ultrafast Innovations GmbH, Am Coulombwall 1, 85748 Garching, Germany*
[*]*vladimir.pervak@lmu.de*

Abstract: We report the utilization of the optical Kerr effect in multilayer dielectric coatings, previously discussed only theoretically. We present the design and realization of multilayer dielectric optical structures with layer-specific Kerr nonlinearities, which permit tailoring of the intensity-dependent effects. The modulation depth in reflectance reaches up to 6% for the demonstrated examples of dielectric nonlinear multilayer coatings. We show that the nonlinearity is based on the optical Kerr effect, with the recovery time faster than the laser pulse envelope of 1 ps. Due to high flexibility in design, the reported dielectric nonlinear multilayer coatings have the potential to open hitherto unprecedented possibilities in nonlinear optics and ultrafast laser applications.

References and links

1. R. W. Boyd, *Nonlinear Optics,* 3rd ed. (Academic Press, 2007).
2. M. A. Duguay and J. W. Hansen, "An ultrafast light gate," Appl. Phys. Lett. **15**(6), 192–194 (1969).
3. D. E. Spence, P. N. Kean, and W. Sibbett, "60-fsec pulse generation from a self-mode-locked Ti:sapphire laser," Opt. Lett. **16**(1), 42–44 (1991).
4. O. Razskazovskaya, T. T. Luu, M. Trubetskov, E. Goulielmakis, and V. Pervak, "Nonlinear absorbance in dielectric multilayers," Optica **2**(9), 803–811 (2015).
5. C. Rodríguez, S. Günster, D. Ristau, and W. Rudolph, "Frequency tripling mirror," Opt. Express **23**(24), 31594–31601 (2015).
6. K. Starke, D. Ristau, H. Welling, T. V. Amotchkina, M. K. Trubetskov, A. A. Tikhonravov, and A. S. Chirkin, "Investigations in the nonlinear behavior of dielectrics by using ultrashort pulses," Proc. SPIE **5273**, 501–514 (2004).
7. W. Chen and D. L. Mills, "Optical response of nonlinear multilayer structures: Bilayers and superlattices," Phys. Rev. B Condens. Matter **36**(12), 6269–6278 (1987).
8. E. Lidorikis, Q. Li, and C. M. Soukoulis, "Wave propagation in nonlinear multilayer structures," Phys. Rev. B Condens. Matter **54**(15), 10249–10252 (1996).
9. L. Brzozowski and E. H. Sargent, "Optical signal processing using nonlinear distributed feedback structures," IEEE J. Quantum Electron. **36**(5), 550–555 (2000).
10. P. K. Kwan and Y. Y. Lu, "Computing optical bistability in one-dimensional nonlinear structures," Opt. Commun. **238**(1–3), 169–175 (2004).
11. N. Moshonas, G. K. Pagiatakis, P. Papagiannis, S. P. Savaidis, and N. A. Stathopoulos, "Simulation and properties of highly nonlinear multilayer optical structures using the transmission line method," Proc. SPIE **9131**, 913129 (2014).
12. R. Adair, L. L. Chase, and S. A. Payne, "Nonlinear refractive index of optical crystals," Phys. Rev. B Condens. Matter **39**(5), 3337–3350 (1989).
13. V. Dimitrov and S. Sakka, "Linear and nonlinear optical properties of simple oxides. 2," J. Appl. Phys. **79**(3), 1741–1745 (1996).
14. S. A. Akhmanov and S. Y. Nikitin, *Physical Optics* (Clarendon Press, Oxford, 1997).
15. H. A. Macleod, "Basic Theory," in *Thin-Film Optical Filters,* 4th ed. (CRC Press Taylor & Francis Group, 2010).
16. A. Thelen, *Design of Optical Interference Coatings* (New York [etc.]: McGraw-Hill, 1989).
17. A. V. Tikhonravov and M. K. Trubetskov, Optilayer software, *http://www.optilayer.com*.
18. V. Pervak, A. V. Tikhonravov, M. K. Trubetskov, S. Naumov, F. Krausz, and A. Apolonski, "1.5-octave chirped mirror for pulse compression down to sub-3 fs," Appl. Phys. B **87**(1), 5–12 (2007).

19. W. Schneider, A. Ryabov, C. Lombosi, T. Metzger, Z. Major, J. A. Fülöp, and P. Baum, "800-fs, 330-µJ pulses from a 100-W regenerative Yb:YAG thin-disk amplifier at 300 kHz and THz generation in LiNbO₃," Opt. Lett. **39**(23), 6604–6607 (2014).
20. J. Bonse, S. Baudach, J. Kruger, W. Kautek, K. Starke, T. Gross, D. Ristau, W. Rudolph, J. Jasapara, and E. Welsch, "Femtosecond laser damage in dielectric coatings," Proc. SPIE **4347**, 24–34 (2001).
21. A. M. Zukauskas and V. Sirutkaitis, "Nonlinear absorption of ultrashort pulses in HR dielectric mirrors," Proc. SPIE **5991**, 599111 (2005).
22. M. Konuma, Plasma techniques for film deposition, Ph.D. thesis, Alpha Science, Harrow, UK (2005).
23. S. C. Jones, P. Braunlich, R. T. Casper, X. A. Shen, and P. Kelly, "Recent progress on laser-induced modifications and intrinsic bulk damage of wide-gap optical-materials," Opt. Eng. **28**(10), 1039–1068 (1989).
24. S. Guizard, P. Martin, G. Petite, P. D'Oliveira, and P. Meynadier, "Time-resolved study of laser-induced colour centres in SiO₂," J. Phys. Condens. Matter **8**(9), 1281–1290 (1996).
25. M. Mero, B. Clapp, J. C. Jasapara, W. Rudolph, D. Ristau, K. Starke, J. Kruger, S. Martin, and W. Kautek, "On the damage behavior of dielectric films when illuminated with multiple femtosecond laser pulses," Opt. Eng. **44**(5), 051107 (2005).
26. I. B. Angelov, A. von Conta, S. A. Trushin, Z. Major, S. Karsch, F. Krausz, and V. Pervak, "Investigation of the laser-induced damage in dispersive coatings," Proc. SPIE **8190**, 81900B (2011).
27. M. Mero, A. J. Sabbah, J. Zeller, and W. Rudolph, "Femtosecond dynamics of dielectric films in the pre-ablation regime," Appl. Phys., A Mater. Sci. Process. **81**(2), 317–324 (2005).
28. J. Hsu, C. Fuentes-Hernandez, A. R. Ernst, and B. Kippelen, "Ultrafast nonlinear mirrors with broad spectral and angular bandwidths in the visible spectral range," Opt. Express **21**(3), 3573–3581 (2013).
29. D. Ristau, H. Ehlers, T. Gross, and M. Lappschies, "Optical broadband monitoring of conventional and ion processes," Appl. Opt. **45**(7), 1495–1501 (2006).
30. W. H. Knox, N. M. Pearson, K. D. Li, and C. A. Hirlimann, "Interferometric measurements of femtosecond group delay in optical components," Opt. Lett. **13**(7), 574–576 (1988).
31. T. V. Amotchkina, A. V. Tikhonravov, M. K. Trubetskov, D. Grupe, A. Apolonski, and V. Pervak, "Measurement of group delay of dispersive mirrors with white-light interferometer," Appl. Opt. **48**(5), 949–956 (2009).
32. O. Pronin, J. Brons, C. Grasse, V. Pervak, G. Boehm, M. C. Amann, V. L. Kalashnikov, A. Apolonski, and F. Krausz, "High-power 200 fs Kerr-lens mode-locked Yb:YAG thin-disk oscillator," Opt. Lett. **36**(24), 4746–4748 (2011).
33. I. B. Angelov, *Development of high-damage threshold dispersive coatings*, Ph.D. thesis, Ludwig-Maximilian University, Munich (2014).
34. C. W. Luo, Y. T. Wang, F. W. Chen, H. C. Shih, and T. Kobayashi, "Eliminate coherence spike in reflection-type pump-probe measurements," Opt. Express **17**(14), 11321–11327 (2009).
35. Z. Vardeny and J. Tauc, "Picosecond coherence coupling in the pump and probe technique," Opt. Commun. **39**(6), 396–400 (1981).
36. B. S. Wherrett, A. L. Smirl, and T. F. Boggess, "Theory of degenerate four-wave mixing in picosecond excitation-probe experiments," IEEE J. Quantum Electron. **19**(4), 680–690 (1983).
37. S. L. Palfrey and T. F. Heinz, "Coherent interactions in pump-probe absorption-measurements – the effect of phase gratings," J. Opt. Soc. Am. B **2**(4), 674–679 (1985).
38. G. Cerullo, C. Manzoni, L. Lüer, and D. Polli, "Time-resolved methods in biophysics. 4. broadband pump-probe spectroscopy system with sub-20 fs temporal resolution for the study of energy transfer processes in photosynthesis," Photochem. Photobiol. Sci. **6**(2), 135–144 (2007).
39. J. Franc, N. Morgado, R. Flaminio, R. Nawrodt, I. Martin, L. Cunningham, A. Cumming, S. Rowan, and J. Hough, "Mirror thermal noise in laser interferometer gravitational wave detectors operating at room and cryogenic temperature," Tech. rep., General Relativity and Quantum Cosmology (2009).

1. Introduction

Dielectric multilayer coatings are fundamental to almost all kinds of laser systems and have therefore significantly contributed to progress in optics. High-power lasers, for example, heavily rely on highly-reflective mirrors. Control of pulse phase properties by dispersive multilayer mirrors (also known as chirped mirrors) is commonly used in ultrafast lasers and applications. The design of the dielectric coatings enables a highly flexible control of almost the entire range of linear optical properties, such as reflectance, bandwidth, phase and dispersion.

Nonlinear optics, however, is still mostly based on bulk materials with mm-sized dimensions. A prominent mechanism is the optical Kerr effect, which can be viewed as an intensity-dependent change of refractive index. Two technologically important consequences of the Kerr effect are self-focusing, used for laser mode-locking, and self-phase modulation, used for compressing laser pulses to few-cycle duration. The quasi-instantaneous response

time of several femtoseconds of the Kerr effect is essential for both applications [1]. Adopting the optical Kerr effect for laser technology has enabled a plethora of ultrafast applications, ranging from the ultrafast light gate [2] to the revolutionary Kerr-lens mode-locking technique [3], from near-at-hand light modulators, presented here, to potential optical-to-optical computers. Previous implementations of nonlinear multilayer mirrors comprised of dielectric materials have not been based on the Kerr effect, but rather relied on nonlinear absorption [4], or frequency conversion [5]. However, a lossless element is essential for many applications, in particular within lasers or enhancement cavities. To this end, dielectric oxide films with low losses (in contrast to metals) come into sight as promising sources of nonlinearity. Moreover, dielectric materials are appealing as they are highly resistant to laser damage, can excellently withstand abrasion and environmental influence, as well as due to the maturity of available deposition technologies.

In this work, we realize *dielectric optical coatings* with nonlinear behavior dominated by the optical Kerr effect, in order to produce a device with almost instantaneous nonlinearity and, preferably, low losses. This idea has not, to date, transcended theoretical investigations [6]. In many simulations foreshowing a strong nonlinear response of dielectric multilayer structures, authors have used materials (often not specified) with overestimated values for Kerr coefficients [7–11]. In reality, the fundamental challenges emerge from the comparatively small nonlinear indices of dielectric materials [1,12,13] and the necessity to work at high intensities. Here, we present the design guidelines for creating multilayer structures in which the overall optical response is made extremely sensitive to slight changes of the layer refractive indices. The result is a Kerr-effect-driven dielectric multilayer element with intensity-dependent reflectance and transmittance. Specifically, reflectance increases at higher intensities, making the device potentially useful for mode-locking applications. This result holds the prospect for devices purely based on dielectric materials and the optical Kerr effect—nonlinear multilayer coatings (NMCs)—allowing nearly-lossless operation for future applications.

2. Materials and methods

2.1 Design considerations

In contrast to all previous works, the present paper is concerned primarily with multilayer dielectric coatings for the near-infrared spectral region (namely 1030 nm) operating at high intensities on the order of 10^9 W/cm^2, leaving semiconductor, organic, metal and exotic materials outside the scope of this study.

The optical Kerr effect in a medium results in an almost instantaneously occurring intensity-induced change in the refractive index [14]:

$$n = n_0 + n_2 \cdot I. \tag{1}$$

Here n_0 is the linear refractive index, n_2 [cm^2/W] is the second-order nonlinear refractive index (often referred to as the Kerr coefficient), and I [W/cm^2] is the light intensity. For example, a light intensity of about 10^9 W/cm^2 can cause observable nonlinearities [14]. A typical response time for the nonlinearity induced by the electronic polarization is 1 fs (ref [1].). In order to enhance the impact of the optical Kerr effect, the optical characteristics of an NMC design need to be sensitive to slight changes in refractive index. An edge filter design, shown in Fig. 1, is extremely sensitive to small refractive index variations in the transition zone between high and low reflectance around 1030 nm (Fig. 1(b)). The Abeles matrix method [15], derived directly from Maxwell's equations and commonly used for calculating the optical properties of multilayers, for a given wavelength λ determines the initial reflectance R_i of an m-layer structure through the physical thicknesses of the layers $d_1, \dots d_m$, and the angle of incidence (AOI) ϑ:

$$R_i = R(d_1, \ldots, d_m; n_H, n_L; \lambda; \vartheta), \tag{2}$$

where n_H and n_L are the refractive indices of the high-index and low-index materials comprising the multilayer stack, respectively. In simplified form, the optical Kerr effect in multilayer coatings can be described as follows. The incident laser beam interferes with itself in the multilayer structure and, consequently, manifests a standing wave distributed along the coordinate perpendicular to the coating surface. Due to the presence of such a standing wave, a weak increase in layer refractive indices corresponding to the field intensity profile emerges, in accordance with Eq. (1). The latter can also be considered as an additional microstructure, which in turn leads to an increase in reflectance of the whole multilayer structure from R_i at low intensities up to its final value R_f at higher intensities:

$$R_f(I) = R_i + \Delta R(I), \tag{3}$$

where $\Delta R(I)$ is the modulation depth of an NMC (see Fig. 1(b)).

The first realization of an NMC (F502) shown in Fig. 1 (low intensity) with a central wavelength of 1030 nm consisted of 69 alternating layers of the dielectric materials Nb_2O_5 (band gap $E_g \sim 3.5$ eV) and SiO_2 ($E_g \sim 8.3$ eV), resulting in a total thickness of 8.7 μm. The working range of the edge filter design is the edge itself (Fig. 1(b)), the position of which can be easily adjusted by varying the AOI of the incident light [16]. The design of F502 was therefore tailored for a non-zero AOI = 20° for p-polarized light. The next realization of an NMC, F504 was obtained with the dielectric materials Ta_2O_5 ($E_g \sim 3.8$ eV) and SiO_2, with a total thickness of 9.3 μm. The multilayer structure of F504 was designed to have an optimized flat group delay dispersion of −5000 fs^2, essential for potential laser applications, at an AOI = 20° over a wavelength range 1024–1033 nm. A commercial software package OptiLayer [17] was used to obtain these designs.

Thorough studies of the nonlinear refractive indices of the dielectric thin-films used in this work have, to date, not been presented in the available literature. However, the nonlinear indices of Nb_2O_5 and Ta_2O_5 in crystal form are on the order of 10^{-15} cm^2/W (refs [12,13].) and are, at times, used for reference purposes.
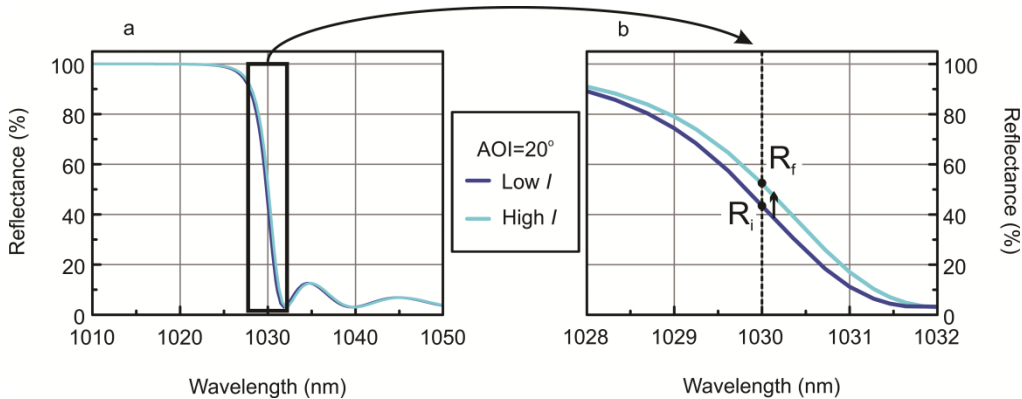

Fig. 1. The optical Kerr effect illustration: **(a)** NMC design F502 over a wide wavelength range; **(b)** NMC design F502 in the vicinity of 1030 nm: Reflectance at the edge increases from R_i at low intensities to R_f at higher intensities.
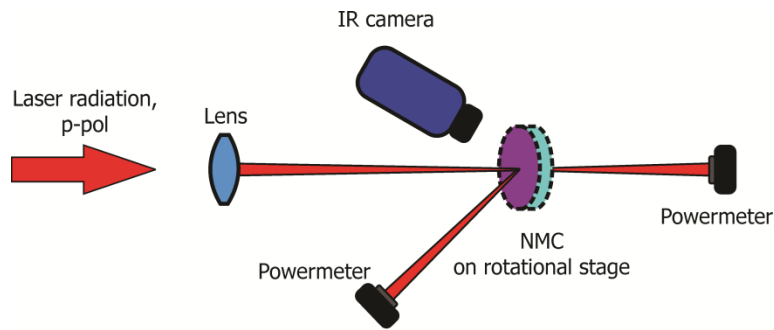
Fig. 2. Schematic of the setup for investigating the pre-damage behavior of the samples. Yb:YAG thin-disk regenerative amplifier: 1030 nm central wavelength, 50 kHz repletion rate, 1 ps pulse duration.

2.2 Sample fabrication and characterization

The designed multilayer structures were deposited on fused silica substrates with thicknesses of 145 μm and 6.35 mm by use of the magnetron sputtering technique [18] (see Appendix A). The pre-damage behavior of the NMCs F502 and F504 coated on 145 μm-thick substrates was studied experimentally with the setup shown in Fig. 2. The laser was an Yb:YAG thin-disk regenerative amplifier with a repetition rate of 50 kHz (ref [19].). The pulse intensity was varied with a half-wave plate followed by a polarization cube placed in front of the focusing lens. A strong escalation of the scattered light from the sample surface, monitored with a charge-coupled device camera, served as an indication of damage occurrence [20]. The laser beam was focused on a sample in order to provide intensities up to 5% below the laser-induced damage threshold of the samples.

Both the reflected and transmitted average power values were measured for each incident power value with a powermeter (PM-10, COHERENT). The relative temperature change of the sample was monitored during the measurements via an IR camera (FLIR SC 300 Series camera A325) with a measurement accuracy of ± 2°C. The IR camera realized an additional control in monitoring damage occurrence, as the relative temperature increased rapidly at the onset of damage. The IR camera was set to measure the temperature difference *ΔTemp* between the spot where the laser hit the NMC sample surface and the ambient medium. The sample was placed on a rotational stage in order to adjust the AOI and achieve different initial reflectance R_i to initial transmittance T_i ratios (R_i/T_i).

Pump-probe measurements were carried out in order to investigate the time response of the NMCs. The experiments were performed with a conventional degenerative pump-probe setup utilizing the aforementioned laser source (see Appendix B).

3. Results and discussion

3.1 Nonlinear pre-damage behavior

Figures 3 and 4 illustrate the pre-damage performance of the NMCs F502 (Nb_2O_5/SiO_2) and F504 (Ta_2O_5/SiO_2) carried out using the setup shown in Fig. 2. The plots reveal evidence that the reflectance of both samples increases, the transmittance decreases and the relative temperature grows with the incident intensity; the total losses (100%–R–T) are on the scale of measurement error.

The observed temperature growth could be justified by absorption, inevitable even in multilayers of high quality [21]. The absorption origin lies outside the present discussion, however, among the possible causes the following might be important: multiphoton absorption, dust particles and impurities, native defects [22] (shallow traps), self-trapped excitons (deep traps) subsequently leading to long-lived color center formations [23–25], or a complex combination thereof. At intensities on the order of 10^9 W/cm², absorption processes

become relevant and result in the temperature increase. However, the extent to which the absorption contributes to the total losses is not quantifiable as the latter lie within the measurement error (Figs. 3 and 4), which allows one to conclude that absorption is not the dominant process in the present case. On the other hand, the modulation depths for both F502 and F504, both in reflectance and in transmittance, are well-defined and are certainly larger than the errors (Figs. 3 and 4).

The modulation depths of the NMCs are determined by the AOI (according position of the edge), which also defines the initial proportion R_i/T_i. As one can see (Figs. 3 and 4), the modulation depths in reflectance and transmittance are much higher for the case $R_i/T_i = 50/50$ (left panels) compared to those at $R_i/T_i = 80/20$ (right panels), for both F502 and F504. It is evident, that the optical properties of the edge filter design are highly responsive to an intensity increase, and ΔR can reach 16% under particular conditions (for $R_i/T_i = 50/50$). Note, that the damage threshold of Nb_2O_5/SiO_2 coatings is usually lower compared with that of Ta_2O_5/SiO_2 coatings [26], which is the case for the results presented here as well (Figs. 3 and 4, compare the last measurement points).

3.2 Decoupling of the temperature influence

As a temperature rise of the NMCs irradiated by a laser was observed (see Figs. 3 and 4), studies were conducted in order to analyze the influence of temperature on the NMC performance. For the presented NMC design, due to thermal expansion and the thermo-optic effect, a temperature rise unavoidably causes a shift of the edge position to longer wavelengths, i.e. in the same direction as the optical Kerr effect (see Fig. 1). Essentially, the steeper the edge of the NMC (enhancing the Kerr effect), the more susceptible it is to temperature shifts. The dependence of ΔR on $\Delta Temp$ was estimated by simultaneously recording reflectance spectra and measuring the surface temperature of the NMCs (coated on 6.35 mm substrates) via an IR camera. This dependence was found to be linear and allows one to separate the temperature impact resulting in the increase in reflectance of the NMCs (for more details see Appendix C).

In order to experimentally exclude the impact of temperature on the NMCs, a chopper wheel was introduced into the setup described above (behind the lens, Fig. 2). When the laser beam is modulated by the chopper wheel (10% duty cycle), the incident average power drops by approximately a factor of ten (as well as the induced temperature modulation) while the incident intensity remains the same.
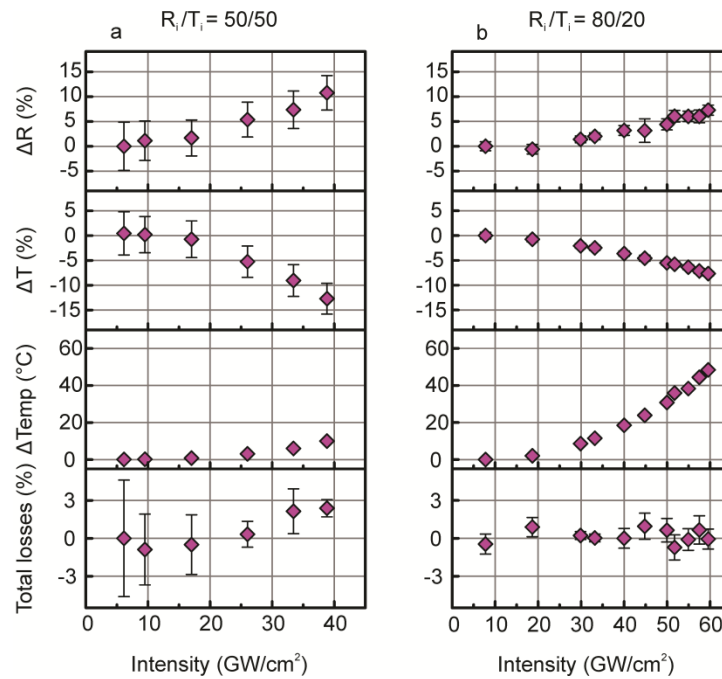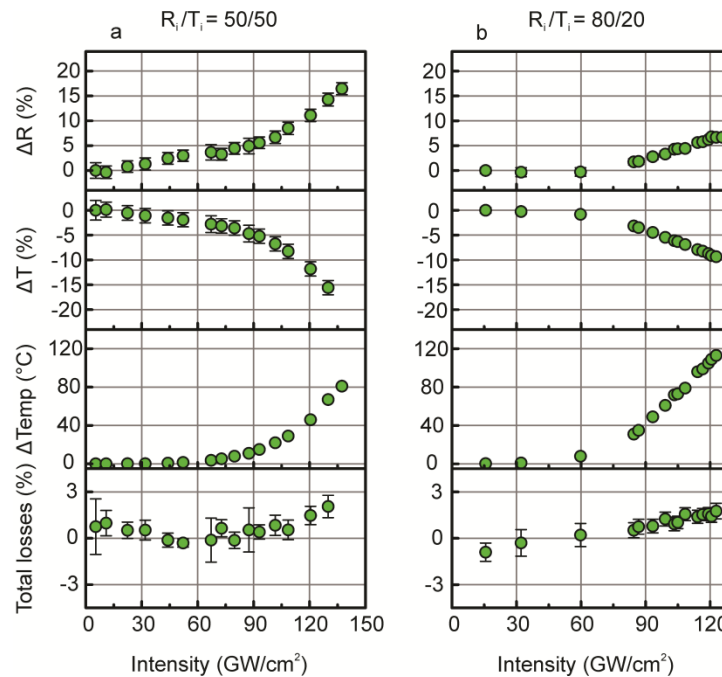
Fig. 3. Intensity-dependent change of reflectance, transmittance, relative temperature and total losses of NMC F502 for R_i/T_i of 50/50 **(a)** and 80/20 **(b)**. The error bars represent standard deviations.

Fig. 4. Intensity-dependent change of reflectance, transmittance, relative temperature and total losses of NMC F504 for R_i/T_i of 50/50 **(a)** and 80/20 **(b)**. The error bars represent standard deviations.

Figure 5 shows the decoupling of the temperature-induced and nonlinear behavior for F502 obtained using the setup shown in Fig. 2 with the incorporated chopper wheel. The

temperature-induced modulation depths ΔR_{temp} for F502 (red triangles in Fig. 5) were computed with the help of the experimentally determined linear slope of the dependence of ΔR on $\Delta Temp$, mentioned above. Next, these ΔR_{temp} estimations were subtracted from both the modulation depths measured with the chopper ΔR_{ch} (blue diamonds in Fig. 5(b) and 5(d)) and the total modulation depths measured without the chopper ΔR_{tot} (violet diamonds in Fig. 5(a) and 5(c)). Thus, the nonlinear change in reflectance ΔR_{nl} was obtained as follows:

$$\Delta R_{nl} = \Delta R_{tot} - \Delta R_{temp}^{tot} \text{ or } \Delta R_{nl} = \Delta R_{ch} - \Delta R_{temp}^{ch}, \tag{4}$$

where ΔR_{temp}^{ch} and ΔR_{temp}^{tot} are the temperature-induced modulation depths with and without the chopper respectively. Analogous estimations were performed for F504 and yield similar results (Fig. 6). The negative values seen in Figs. 5 and 6 can be vindicated by an increased error budget of the powermeter at low intensities. Finally, the "pure" nonlinear changes estimated in this manner for both NMCs correspond to the measured values of modulation depths of reflectance in absence of temperature growth within the experimental uncertainty (Figs. 5 and 6).

The temperature impact appears to be almost 50% (or even more depending on the value of R_i/T_i) of the observed modulation depths in reflectance and transmittance for the unmodulated laser radiation case (chopper off in Figs. 5 and 6). Basically, the experimentally observed pre-damage behavior of the studied elements is an interplay between the temperature-induced and nonlinear effects in these particular NMC realizations. Nevertheless, it is possible to circumvent the temperature influence by introducing a chopper wheel. Thus, the modulation depths measured in such a way can be regarded as "pure" nonlinear effect estimations. As one can notice, the effect of about 6% occurs at 50% edge of the filter F504 (Fig. 6), and the effect of about 3% – at 80% of the same edge filter. These values can be concluded to be rather large if to take into consideration that the nonlinear coefficients of dielectrics are estimated to be on the order of 10^{-15} cm^2/W (refs [12,13].) and a typical change in refractive index is not higher than 0.01.
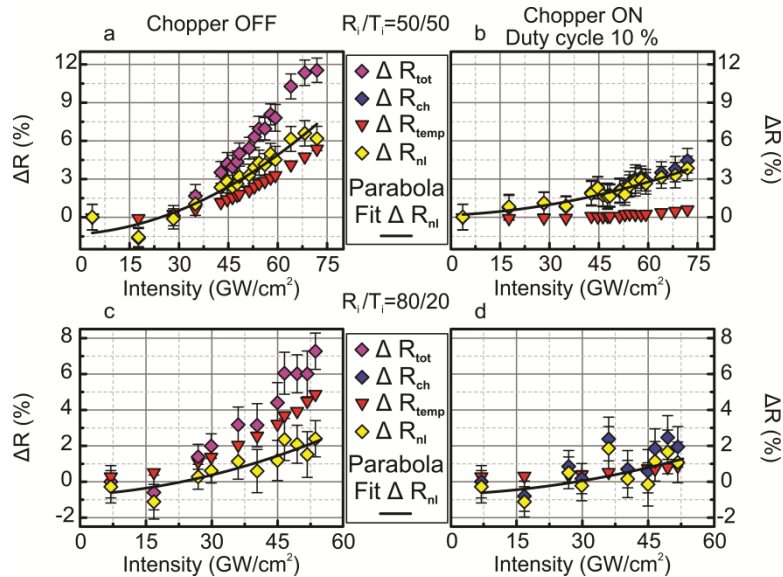

Fig. 5. Estimation of the "pure" nonlinear effect for NMC F502: Estimated nonlinear ΔR_{nl} (yellow diamonds) is obtained as a result of subtraction of the temperature-induced ΔR_{temp} (red triangles) from the measured ΔR_{tot} (**a, c**: violet diamonds) without chopper and ΔR_{ch} (**b, d**: blue diamonds) with chopper for two cases of R_i/T_i of 50/50 (upper panels **a** and **b**) and 80/20 (lower panels **c** and **d**). The error bars represent standard deviations. Parabola fits (solid black curves) serve as a guidance to the eye.
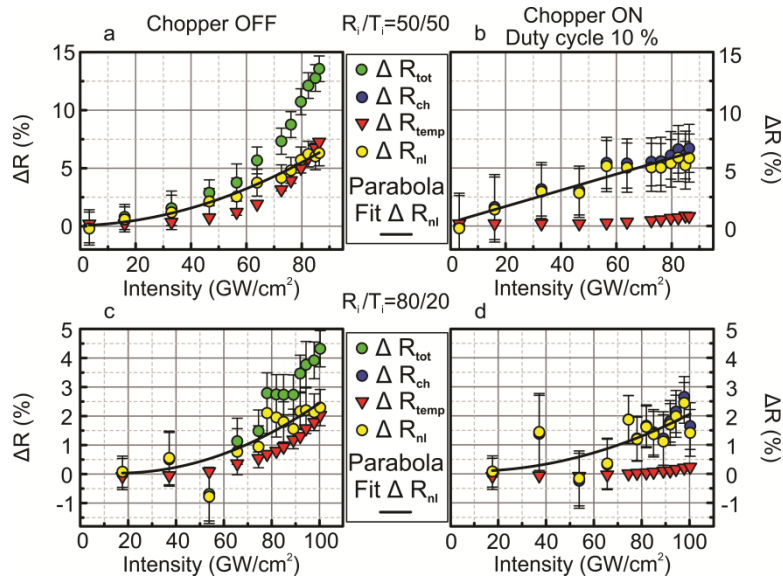
Fig. 6. Estimation of the "pure" nonlinear effect for NMC F504: Estimated nonlinear ΔR_{nl} (yellow circles) is obtained as a result of subtraction of the temperature-induced ΔR_{temp} (red triangles) from the measured ΔR_{tot} (**a, c**: green circles) without chopper and ΔR_{ch} (**b, d**: blue circles) with chopper for two cases of R_i/T_i of 50/50 (upper panels **a** and **b**) and 80/20 (lower panels **c** and **d**). The error bars represent standard deviations. Parabola fits (solid black curves) serve as a guidance to the eye.

3.3 Pump-probe measurements

Pump-probe measurements were performed in order to fully verify the Kerr-based nature of the nonlinear response of the new elements. Time-resolved recovery curves of the NMCs F502 and F504 for different values of R_i/T_i, obtained with a conventional pump-probe setup, are presented in Fig. 7, panels a and b respectively. Any possible coherence spike, typically observed near zero delay time at about 5–20 fs (see for example ref [27].), cannot be resolved due to the much longer source pulse duration of 1 ps. The detected relative changes of R are presented normalized as these values are most probably affected by the presence of the coherence spike, and thus are not of interest. Note also, that pump-probe technique was used in order to measure the time response of the NMCs, not the absolute values of the modulation depth in reflectance. Figures 7 and 8 provide evidence that the reflectance change disappears very quickly after the pump pulse for both initial conditions. Over the course of the measurements, the recovery of F504 was consistently below the 1 ps sensitivity of the detection system. The response time of F502, however, contained some features observed after the pump pulse is gone (Fig. 7). These undetermined features are under ongoing investigation.

The autocorrelation function (ACF) of the laser source used in the experiments was measured with the help of a commercial autocorrelator (A·P·E pulseCheck 15). The measured ACF was then fitted by the expected Gaussian function with a full width at half maximum (FWHM) of 1.46 ps, from which the pulse duration τ_p of 1 ps can be calculated via $\tau_p = \frac{1}{\sqrt{2}} \cdot FWHM$. The normalized time response of both NMCs is compared to the Gaussian fitted ACF (solid black curves in Figs. 7 and 8). Panels b and d in Fig. 8 make it obvious that the recovery of F504 entirely follows the 1-ps pulse. Much slower temperature effects, usually occurring within seconds, cannot contribute to response of NMCs on 1 ps time scale. Thus, at least for F504, the "pure" change in reflectance measured previously (Fig. 6) is fully related to the nonlinear time response with an upper limit of 1 ps. For comparison,

the nonlinear response of a metallodielectric mirror [28] does not fully recover after a delay of 16 ps.
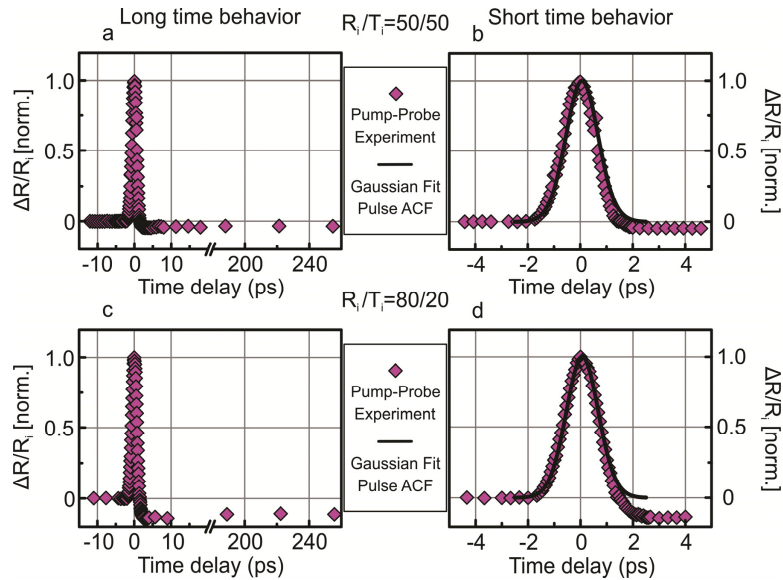

Fig. 7. Normalized time response of NMC F502, hit by a 1-ps pulse at zero time delay for two cases of R_i/T_i of 50/50 (upper panels **a** and **b**) and 80/20 (lower panels **c** and **d**). Left panels **a** and **c** illustrate the long time behavior, whereas right panels **b** and **d** illustrate the short time behavior. Solid black curves are Gaussian fitted ACF.
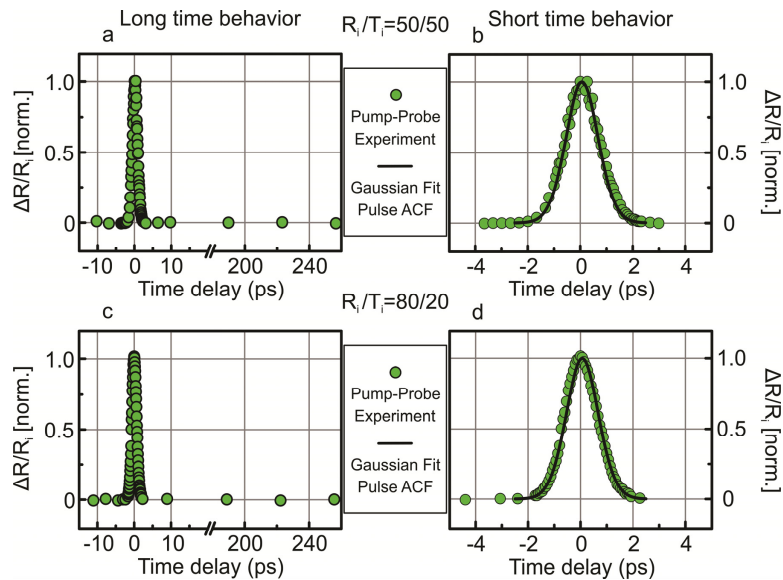

Fig. 8. Normalized time response of NMC F504, hit by a 1-ps pulse at zero time delay for two cases of R_i/T_i of 50/50 (upper panels **a** and **b**) and 80/20 (lower panels **c** and **d**). Left panels **a** and **c** illustrate the long time behavior, whereas right panels **b** and **d** illustrate the short time behavior. Solid black curves are Gaussian fitted ACF.

Overall, in multilayer thin films, nonlinear absorption has been shown to only lead to decreasing reflectance (e.g., ref [4].), which is not the case in the present study (Figs. 3 and 4). The temperature-induced effects were isolated, enabling the observation of the "pure" nonlinear effect (Figs. 5 and 6). Recovery of the NMCs with an upper limit of 1 ps was shown

(Fig. 8). Hence, from a physical point of view, the nonlinear pre-damage performance of the NMCs is dominated by the optical Kerr effect. Previously reported calculations [6,9,11] and experiments with various nonlinear optical devices (e.g., refs [5,28].) have predominantly been performed for the wavelengths equal to or shorter than 800 nm, where multiphoton absorption processes arise in dielectrics with a high probability. For the present investigation, any multiphoton absorption processes are considered detrimental. For the same bandgap, the longer the wavelength, the less the probability of multiphoton absorption and other intensity-dependent absorption effects, hindering the beneficial optical Kerr effect. A step towards longer wavelengths and, consequently, to a nonlinear optical response dominated solely by the optical Kerr effect, was undertaken herein. Operating at longer wavelengths such as 1.5 μm or 2 μm is expected to bypass the limitations originating from intensity-dependent absorption.

3.4 Possible applications

Here, one of the possible applications is demonstrated, namely performance of an NMC as a passive, intensity-stabilizing element for laser pulse trains. Figure 9 shows a plot of average transmitted power versus incident laser peak intensity, illustrating that the transmitted power practically remains constant in the nonlinear regime (starting from about 100 GW/cm^2) despite the increasing incident intensity. This result shows that NMC F504 exhibits "limiting performance", i.e., limits the transmitted power to a certain value which depends on the R_i/T_i ratio. The instantaneous Kerr effect thereby ensures fast stabilization of the transmitted radiation, whereas the temperature effect additionally provides slow stabilization at a time scale of 1 s.
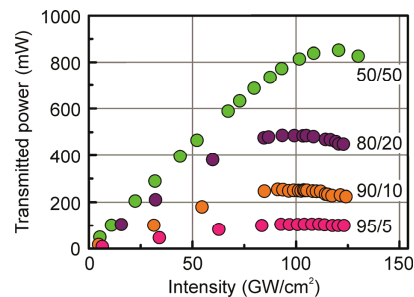

Fig. 9. Limiting performance of NMC F504: Dependence of transmitted power on the peak intensity for different R_i/T_i values enumerated by the legend.

4. Conclusions

Nonlinear multilayer coatings (NMCs) for the near-infrared spectral range have been designed, manufactured and characterized in detail within the frame of this work. The observed behavior of the NMCs has been found to be the result of two separate manifestations: a quasi-instantaneous nonlinear response driven by the optical Kerr effect, and temperature-induced effects arising through thermal expansion and the thermo-optic effect. The detrimental temperature influence has been studied independently. The modulation depth in reflectance of the NMCs due to the optical Kerr effect has been shown to be as high as 6%, which is fairly significant considering the small Kerr coefficients of the composing dielectric materials. Pump-probe measurements have shown that the nonlinearity of the NMCs has a rapid recovery time shorter than the laser envelope width of 1 ps.

It can be realistically conceived that dielectric NMC elements, which can be fabricated using standard coating techniques available in many facilities around the world, could become a substantial alternative for conventional nonlinear materials in laser applications. NMCs can potentially be integrated in laser oscillators as intensity-limiting, spatial or

temporal filters. With further optimization, NMCs may serve as multilayer amplitude modulators for initiating or assisting laser mode-locking.

Appendix

A. Deposition technique and post-production characterization

The designed nonlinear multilayer coatings (NMCs) were produced by means of the coating plant (Helios, Leybold Optics) equipped with two proprietary TwinMags magnetrons and a plasma source for plasma/ion-assisted reactive middle-frequency dual-magnetron sputtering. It exploits precise time-controlled monitoring of layer thicknesses, based on accurate calibration of the deposition process parameters affecting deposition rates. Additionally, built-in broadband in-situ monitoring [29] with a B270 test glass as a witness sample was used.

After production, the samples were characterized with the help of a commercial spectrophotometer (Perkin Elmer Lambda 950) and a home-built white-light interferometer [30,31]. A comparison between the designed and measured data is presented in Fig. 10. The agreement between theoretical and experimental data is quite good, given that the design is rather sensitive to manufacturing errors. However, some deviation, that can be noticed in Fig. 10(b), is not important as it can be easily compensated for by tuning the angle of incidence (AOI) of the incident light at an NMC.

It should be mentioned, that peak powers not higher than 75 MW (average power 4 W) were used for sample characterization, and the beam waste w at the sample was rather large (about 180 μm). On the other hand, many systems operate at lower intracavity peak powers of 5–40 MW (ref [32].) requiring much tighter focusing, which may cause self-focusing over the 6.35-mm propagation distance of a standard fused silica substrate. In such thick substrates, self-focusing processes may alter the properties of the transmitted beam, which is detrimental for the potential laser applications. In order to characterize the potentially applicable laser components, the NMCs deposited on the particular thin (145 μm) substrates were used in the course of measurements with the laser involved. Notice, that the thin (145 μm) substrates cannot be polished as good as standard (6.35 mm) ones, which might justify the reduced damage threshold values.

The peak intensity I_p for a Gaussian pulse, both temporally and spatially in transverse direction, was calculated as follows [33]:

$$I_p = \left(\frac{\pi}{2}\right)^{-\frac{3}{2}} \frac{P}{f_{rep}\tau_p w^2}, \tag{5}$$

where P is the average incident power, f_{rep} is the laser repetition rate (50 kHz), τ_p is the pulse duration (1 ps), and w is Gaussian beam radius – the distance from the beam axis, at which the intensity drops to $1/e^2$ of its maximum value (about 180 μm in this study). Notice also that the intensity values presented in this work should only be used as a guide due to imperfect beam radius estimation.
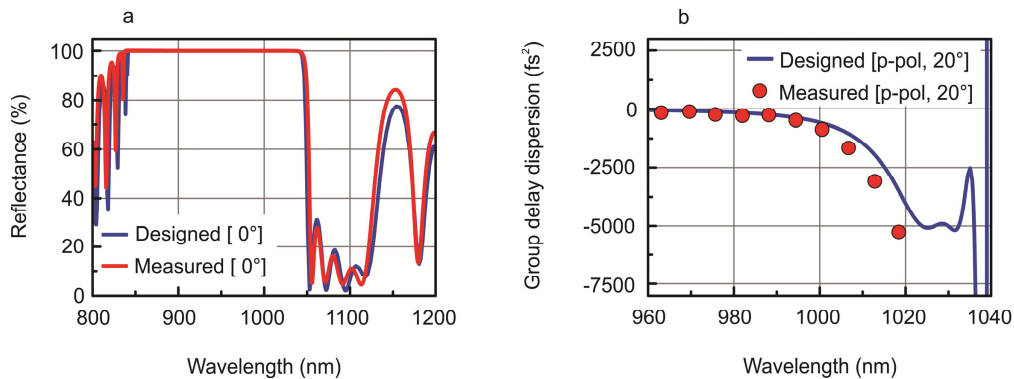
Fig. 10. Comparison of the designed and measured data for NMC F504: **(a)** The designed reflectance (blue curve) and the measured data (red curve) at AOI = 0°; **(b)** The designed group delay dispersion (blue curve) and the measurement performed with a white-light interferometer (red circles) for p-polarized light at AOI = 20°.

B. Pump-probe setup

Figure 11 displays the pump-probe setup used. The incoming pulse was divided by a beam splitter into pump and probe pulses, and the latter was sent through a variable delay line. The probe beam was attenuated by a factor of 100 with respect to the pump in order to measure only the pump-induced reflectance changes.

Both pulse replicas were focused on the sample by lenses, and the reflected probe pulse was detected by a photodiode. To examine an approximately uniformly excited region of the sample, the probe was focused onto a spot significantly smaller than the area of the pump. The probe beam remained s-polarized whereas the polarization of the pump was rotated through 90° after propagating across a half-wave plate and a polarization cube, which decreased the possibility of a pronounced so-called "coherence spike" appearing [34]. Many scientific groups have reported on observing a peak around zero delay time, termed as coherence spike (known as coherent interaction or coherent nonlinearity as well) in pump-probe femtosecond measurements [27, 35–37]. The possible presence of a coherence spike needs to be taken into account, because the measurement results achieved with the pump-probe method may contain artefacts which can falsely be attributed to the sample response.

The photodiode was set to detect s-polarization by employing another half-wave plate and a cube immediately before the detector, hence reducing the influence of unwanted scattered light (Fig. 11). The pump pulse was mechanically modulated by a chopper and the pump-induced reflectance modulation of the probe was detected by a lock-in amplifier in order to increase the signal-to-noise ratio. Typically, this kind of setup is capable of a sensitivity up to $\Delta R/R_i = 10^{-4}$ at 1 kHz (ref [38]).

The linear reflectance R_i (initial reflectance at low intensities) of the samples was measured separately by a powermeter in order to set the desired initial reflectance R_i to initial transmittance T_i ratios (R_i/T_i). The time response measurements of the NMCs were performed at the intensities of approximately 15% below the damage threshold.
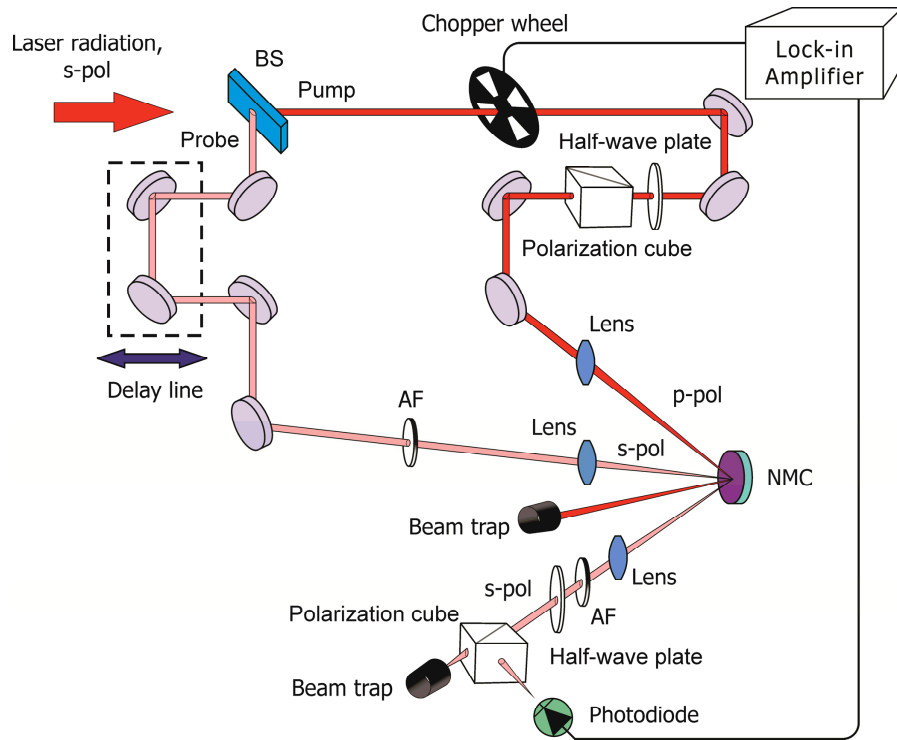
Fig. 11. Schematic of a degenerate pump-probe setup. BS, beam splitter; AF, attenuating filter.

C. Temperature influence estimations

First, NMCs F502 and F504 coated on 6.35 mm fused silica substrates were placed into an oven (for 2-2.5 hours at 100°C and 150°C respectively) and were characterized with the help of the industrial spectrophotometer Perkin Elmer Lambda 950 and a portable FLIR E5 camera. Figure 12 illustrates representative temperature measurements for the NMCs. Both the reflectance spectra and the absolute temperature of the samples were recorded starting from the maximal temperature (red curves in Fig. 12) down to the ambient air temperature (blue curves in Fig. 12). Figure 12 experimentally confirms that a temperature rise leads to a shift of the edge position to longer wavelengths.
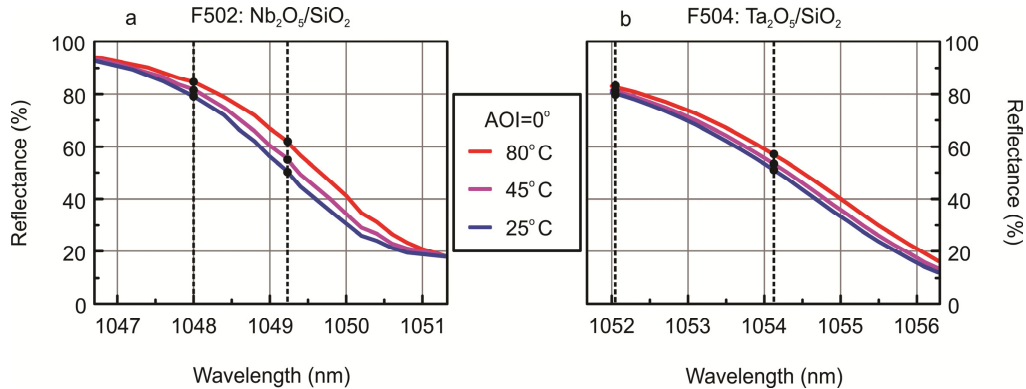

Fig. 12. Reflectance spectra of NMC F502 **(a)** and NMC F504 **(b)**: Spectra shift to longer wavelengths with increasing temperature. Black circles positioned at dashed lines set for two cases of R_i/T_i of 50/50 and 80/20 show the increase of reflectance due to the temperature rise.

Table 1. Thermo-mechanical and optical parameters for the layer materials at room temperature[a]

Layer material	Thermal expansion coefficient α, K^{-1}	Thermo-optic coefficient β: dn/dT
SiO$_2$	0.51×10^{-6}	8×10^{-6}
Ta$_2$O$_5$	3.6×10^{-6}	2.3×10^{-6}
Nb$_2$O$_5$	5.8×10^{-6}	**1.43×10^{-5}**

[a]From ref [39]. and references therein.

For an accurate characterization, it is necessary to determine the evolution of the optical properties of each layer material composing the multilayer stacks in response to a change in temperature. Therefore, knowledge of the physical parameters describing each dielectric material, such as the coefficient of thermal expansion α and the thermo-optic coefficient β is required. Franc et al. have summarized the thermo-mechanical and optical parameters for several optical coating materials (ref [39]. and references therein). The coefficients α and β for the dielectric materials used in this study are shown in Table 1. However, these parameters have mainly been determined for single layers and are in general different for multilayer stacks. Moreover, the coefficients α and β of a single layer always depend on the deposition process. Thus, the coefficients α and β for the NMCs presented here most probably differ from the literature ones. As evident from Table 1, Nb$_2$O$_5$ is more susceptible to temperature than Ta$_2$O$_5$: thermal expansion coefficient for the former is 1.6 times larger, and the thermo-optic coefficient is one order of magnitude higher than that of Ta$_2$O$_5$. One can estimate the change in reflectance due to thermal effects ΔR_{temp}, for a certain temperature change $\Delta Temp$, based on the coefficients of thermal expansion α and the thermo-optic coefficient β for each layer of the m-layer structure:

$$\Delta R_{temp} = R(d_1(1+\alpha_1 \cdot \Delta Temp),\ldots,d_m(1+\alpha_m \cdot \Delta Temp);$$
$$n_H + \beta_H \cdot \Delta Temp, n_L + \beta_L \cdot \Delta Temp; \lambda; \vartheta) - R_i, \tag{6}$$

where $d_1, \ldots d_m$ are the physical thicknesses of the layers, n_H and n_L are the refractive indices of the high-index and low-index materials comprising the multilayer stack, respectively, and ϑ is the AOI.
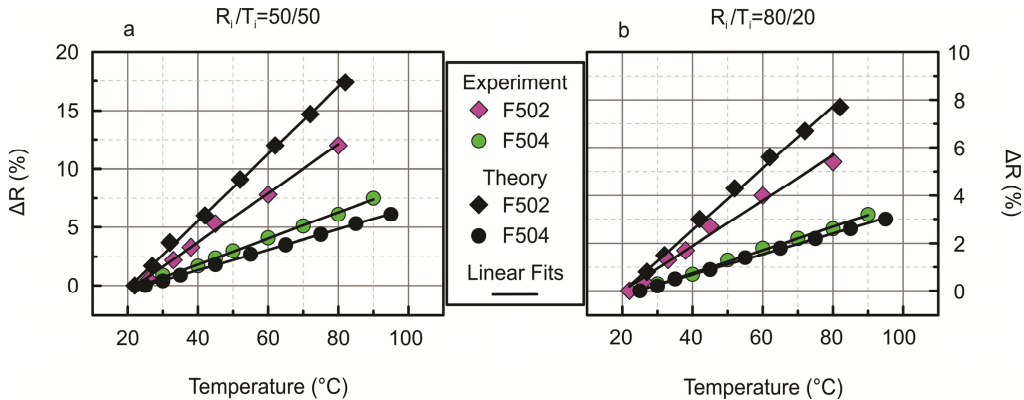

Fig. 13. Comparison of the temperature influence for NMCs F502 and F504 for two cases of R_i/T_i of 50/50 **(a)** and 80/20 **(b)** based on experimental (violet diamonds and green circles, accordingly) and theoretical estimations (black diamonds and circles, accordingly). Solid black lines are linear fits of both experimental and theoretical estimations.

Further, the measured data in Fig. 13 allows one to estimate the dependence of ΔR on the temperature for both NMC samples (violet diamonds for F502 and green circles for F504 in Fig. 13) at two levels of R_i/T_i (50/50 and 80/20). Theoretical estimations for ΔR (black diamonds for F502 and black circles for F504 in Fig. 13) based on the literature coefficients

(Table 1) were computed by virtue of Eq. (6) for the temperature values measured in the experiment at same two levels of R_i.

As indicated in Fig. 13, the theoretical and experimental estimations correlate quite well for NMC F504, while the data for NMC F502 does not quite agree with each other. This discrepancy may be the result of more reliably defined coefficients for Ta_2O_5 thin films compared to those for Nb_2O_5 as more studies have been performed for Ta_2O_5 thin films than for films composed of Nb_2O_5 (see, e.g., ref [39]. and references therein). Furthermore, one can notice, that the sample F504 is less prone to temperature effects than the F502, as it was expected based on the thermal parameters of the comprised materials (Table 1).

Funding

Acknowledgments